The Skill of ECMWF Medium-Range Forecasts during the Year of Tropical Convection 2008

ARINDAM CHAKRABORTY

Divecha Centre for Climate Change, and Centre for Atmospheric and Oceanic Sciences, Indian Institute of Science, Bangalore, India

(Manuscript received 8 September 2009, in final form 24 March 2010)

ABSTRACT

This study uses the European Centre for Medium-Range Weather Forecasts (ECMWF) model-generated high-resolution 10-day-long predictions for the Year of Tropical Convection (YOTC) 2008. Precipitation forecast skills of the model over the tropics are evaluated against the Tropical Rainfall Measuring Mission (TRMM) estimates. It has been shown that the model was able to capture the monthly to seasonal mean features of tropical convection reasonably. Northward propagation of convective bands over the Bay of Bengal was also forecasted realistically up to 5 days in advance, including the onset phase of the monsoon during the first half of June 2008. However, large errors exist in the daily datasets especially for longer lead times over smaller domains.

For shorter lead times (less than 4–5 days), forecast errors are much smaller over the oceans than over land. Moreover, the rate of increase of errors with lead time is rapid over the oceans and is confined to the regions where observed precipitation shows large day-to-day variability. It has been shown that this rapid growth of errors over the oceans is related to the spatial pattern of near-surface air temperature. This is probably due to the one-way air–sea interaction in the atmosphere-only model used for forecasting. While the prescribed surface temperature over the oceans remain realistic at shorter lead times, the pattern and hence the gradient of the surface temperature is not altered with change in atmospheric parameters at longer lead times. It has also been shown that the ECMWF model had considerable difficulties in forecasting very low and very heavy intensity of precipitation over South Asia. The model has too few grids with ''zero'' precipitation and heavy ($>$40 mm day^{-1}) precipitation. On the other hand, drizzle-like precipitation is too frequent in the model compared to that in the TRMM datasets.

Further analysis shows that a major source of error in the ECMWF precipitation forecasts is the diurnal cycle over the South Asian monsoon region. The peak intensity of precipitation in the model forecasts over land (ocean) appear about 6 (9) h earlier than that in the observations. Moreover, the amplitude of the diurnal cycle is much higher in the model forecasts compared to that in the TRMM estimates. It has been seen that the phase error of the diurnal cycle increases with forecast lead time. The error in monthly mean 3-hourly precipitation forecasts is about 2–4 times of the error in the daily mean datasets. Thus, effort should be given to improve the phase and amplitude forecast of the diurnal cycle of precipitation from the model.

1. Introduction

An accurate forecast of precipitation over the South Asian monsoon region at high spatial resolution up to 10 days in advance is necessary for decision making in different areas like agriculture and water resources management. Although significant improvements have been made in short-range forecasting by numerical models during the past few decades (Simmons and Hollingsworth 2002; Harper et al. 2007; Kalnay et al. 1998), there still exists large errors in short-to-medium-range forecasts (e.g., McMurdie and Mass 2004; Wedam et al. 2009). The forecast errors can be associated with errors in the time (phase; Colle et al. 2001) or the intensity in the forecasted parameter (Charles and Colle 2009). A recent study by Wedam et al. (2009) compared the skill of four different operational models to forecast sea level pressure along the east and west coasts of the United States. This study showed that the forecast errors can have significant variation regionally as well as from one model to another.

Corresponding author address: Arindam Chakraborty, Divecha Centre for Climate Change and Centre for Atmospheric and Oceanic Sciences, Indian Institute of Science, Bangalore, 560012, India.
E-mail: arch@caos.iisc.ernet.in

DOI: 10.1175/2010MWR3217.1

Today, many centers all over the world forecast weather on a day-to-day basis using global general circulation models (GCMs). Models used by these centers have various spatial resolution and physics. The lack of high spatial resolution of the global models can perhaps be partially compensated for by the use of mesoscale models. However, performance of mesoscale models also depends on its lateral boundary conditions, which usually come from large-scale model forecasts in real time. Moreover, detailed objective analysis of skill scores and model intercomparison for mesoscale model forecasts tail far behind that of the global model. One of the reasons could be the lack of observations at high spatial resolution in the domain of interest.

The increase in spatial resolution of the models does not necessarily improve the forecast skill. In fact, small phase errors in high spatial and temporal resolution forecasts result in low hit rates and high false alarms. This is termed a double penalty (Anthes 1983; Mass et al. 2002). Moreover, all the physics at small spatial scales are not completely known to implement into a mesoscale model. Furthermore, the simulation time of high-resolution models is quite high and even with present-day computers it is nearly impossible to run a very high-resolution model over a large domain in real time. Downscaling strategy is deployed to overcome some of these issues. This includes statistical and dynamical downscaling of weather and climate forecasts (Druyan et al. 2002; Pandey et al. 2000; Huth 2002; Storch et al. 2000; Krishnamurti et al. 2009; Chakraborty and Krishnamurti 2009). However, useful forecasts of precipitation at a regional level over the Indian summer monsoon region still remain a challenge.

The reason behind these shortcomings could be the errors in the parameterization schemes used in the numerical models and the imperfect initial condition due to lack of good observational data. The increase in model resolution may not result in a better forecast statistics because the parameterization schemes of the models may not be able to resolve all the processes in the high-resolution grid. A detailed analysis of forecasts using high-resolution observation data is thus required to access model error statistics at high spatial resolution.

One important issue that needs to be addressed with high spatial resolution datasets is the diurnal cycle of convection. Although convection, in general, shows an afternoon peak over land and late night to early morning peak over the oceans, there are many exceptions to that general convention. It was shown by Shin et al. (1990) and Janowiak et al. (2005) that phases of precipitation over ocean can occur during afternoon hours. On the other hand, nocturnal maxima in precipitation over the central North American land was noticed (Wallace 1975; Dai et al. 1999). A recent study by Yang and Smith (2006) used the Tropical Rainfall Measuring Mission (TRMM) 3B42 datasets to demonstrate the phase of diurnal cycle of convection can vary both over land and ocean. Even over land, within a small distance the phase of the diurnal cycle can be very different. Murakami (1983) and Krishnamurti et al. (2007) have shown that over the eastern Tibetan Plateau the diurnal peak is in the afternoon hours but a few hundred kilometers south of that at the Himalayan foothills the peak is in the early morning hours. The actual reason for this variation in phase of diurnal cycle is not known. Several observational and modeling studies tried to address this issue (e.g., Bergman 1997; Randall et al. 1991; Dai et al. 1999; Dai 2001). Therefore, it is required to study the characteristics of diurnal cycle in high-resolution observation as well as in the model datasets.

Since May 2008, the World Climate Research Programme (WCRP) and the World Weather Research Programme/The Observing System Research and Predictability Experiment (WWRP/THORPEX) have been organizing coordinated observations, modeling and forecasting organized tropical convection with a goal to better understand its multiscale structure and interaction. This program is titled as the Year of Tropical Convection (YOTC). As a part of this program, the European Centre for Medium-Range Weather Forecasts (ECMWF) is generating high-resolution model forecasts up to 240 h from May 2008 through October 2009. (The details of this project can be obtained online at http://www.ucar.edu/yotc/ and at http://www.wmo.int/pages/prog/arep/wwrp/new/yotc.html.) This study is intended to analyze these high-resolution forecasts from ECMWF over the South Asian monsoon region during June to September 2008 to find out their usefulness and reasons behind shortcomings. This paper is organized as follows. The next section describes the model and the datasets used in this paper. Section 3 outlines the methodology of different analysis used. The results are described in detail in section 4, followed by the major conclusions of this study.

2. Model description and datasets

We have used the ECMWF model forecasts available for the YOTC period. The model is a global atmospheric GCM and uses 799 waves in horizontal with triangular truncation (T799). The equivalent resolution in grid space near the equator is about 0.22°. The model has 91 vertical levels. The ECMWF weather forecast system uses a four-dimensional variational data assimilation system to initialize the model. The datasets available as a part of the YOTC program consists of model forecasts starting at 1200 UTC every day since 1 May 2008. A detailed

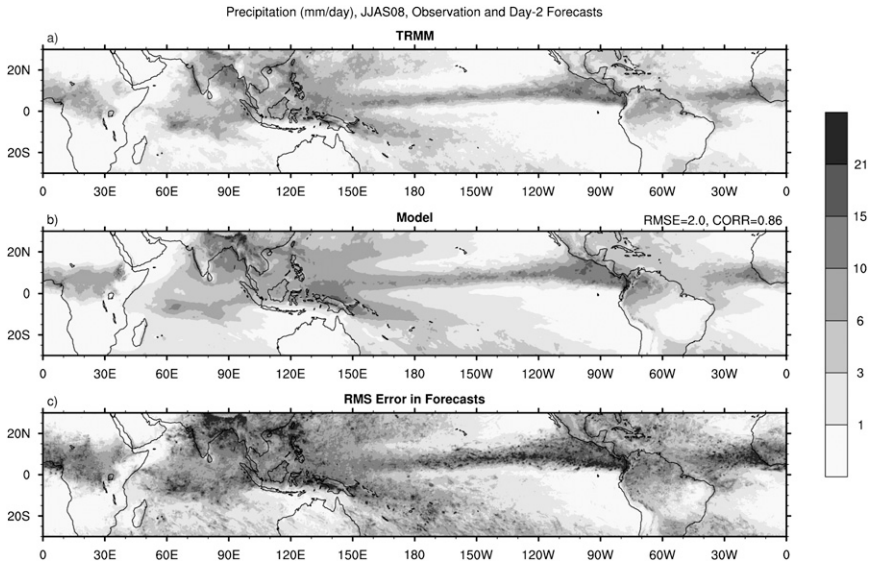

FIG. 1. Precipitation (mm day^{-1}) from (a) TRMM observations, (b) ECMWF forecasts for day 2 averaged over June–September 2008, and (c) RMS errors in ECMWF forecasts in time for the same period. The spatial correlation and RMS error of the mean forecast fields with the TRMM values are indicated as numbers at the top of (b).

description of the model can be found in Bengtsson and Simmons (1983), Simmons and Hollingsworth (2002; also online at http://www.ecmwf.int/products/data/operational_system/evolution). This model outputs are available over 1600 equally spaced grids in east–west and 800 Gaussian grids in north–south directions for the year 2008.

The observational datasets used in this study consists of 3-hourly precipitation from the TRMM 3B42 product. The spatial resolution of this datasets is 0.25°. We had to spatially interpolate the ECMWF model output to that of TRMM equally spaced grid for comparison purposes. Observational datasets for 2-m air temperature was obtained from ECMWF analysis that was available as a part of the YOTC program. No spatial regridding was done on these datasets since they share the same horizontal resolution as the model forecast.

3. Methodology

The ECMWF model starts at 1200 UTC of every day since May 2008 and integration is performed up to 240 h. Model outputs are available at every 3 h up to 96 h from the model start. Outputs are 6-hourly from 96 to 240 h of forecasts. We have averaged all 3-hourly outputs from 0000 through 2100 UTC (and 6-hourly outputs from 0000 through 1800 UTC) to create daily mean datasets from the YOTC model and analysis. Thus, model forecasts averaged over lead times of 12, 15, 18, 21, 24, 27, 30, and 33 h is termed as day-2 forecasts in this study. Longer lead times follow similarly. The string of day-2 forecasts starting at every initial condition during the period 1 May–30 September constitutes the daily time series for this lead time.

To study diurnal cycle (section 4g), initially the 8 time points per day of 3-hourly data were averaged hour by hour over a month to obtain the monthly mean picture of the temporal variation of precipitation during a day. Later, fast Fourier transform was applied to extract the diurnal cycle. This is further discussed in that section.

4. Results

a. Precipitation forecast skills over the tropics

Figures 1 and 2 show the seasonal mean precipitation from TRMM observations and ECMWF model forecasts for days 2 and 5, respectively, during June–September 2008 over the tropics. Also shown, in the bottom panels, is the spatial distribution of root-mean-square (RMS) errors in time for these forecasts. The day-2 forecasts of the model reasonably captured the overall seasonal mean pattern of tropical precipitation. The African tropical convergence zone (TCZ), maxima over Indian Ocean south of the equator near 10°S, orographic maxima at the west coast of India, foothills of the Himalayas and Mayanmar, and north and south components of TCZ over Pacific Ocean were well forecasted by the model (Figs. 1a,b) both in terms of spatial location and extent. However, ECMWF models overestimated precipitation over northeast India, Mayanmar, central Africa, and at

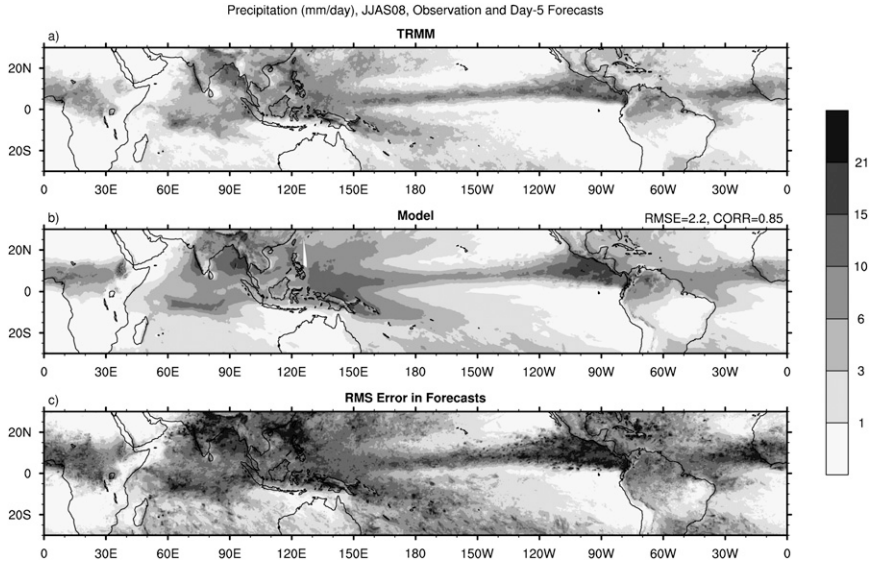

FIG. 2. Precipitation (mm day^{-1}) from (a) TRMM observations, (b) ECMWF forecasts for day 5 averaged over June–September 2008, and (c) RMS errors in ECMWF forecasts in time for the same period. The spatial correlation and RMS error of the mean forecast fields with the TRMM values are indicated as numbers at the top of (b).

the South Pacific convergence zone (SPCZ) region when compared to the TRMM dataset. The RMS error of the seasonal mean forecasts was 2.0 mm day^{-1} and the spatial correlation was 0.86. This RMS error in space was calculated in the following way:

$$\mathrm{RMSE}_s = \sqrt{\frac{\sum_{i,j=1}^{N,M}(M_{i,j} - O_{i,j})^2}{N \times M}}, \qquad (1)$$

where N and M and total number of points in space, and $M_{i,j}$ and $O_{i,j}$ are model and observed fields at ith and jth location. The RMS error in time at a grid (Fig. 1c) was calculated using

$$\mathrm{RMSE}_t = \sqrt{\frac{\sum_{i=1}^{N}(M_i - O_i)^2}{N}}, \qquad (2)$$

where M_i and O_i are forecasted and observed precipitation values at the ith time point, and N is the total number of time points (122 for June–September daily data). This figure shows that even though the model could capture the overall pattern of seasonal mean precipitation over the tropics during June–September 2008, the day-to-day error was very large. In general, errors are larger over regions where mean (Figs. 1a) and standard deviation of observed precipitation are high. The error patterns are very similar during days 2 and 5 of the forecasts (Figs. 1 and 2), but the area mean errors increased from days 2 through 5.

Figure 3 shows the area mean RMSE$_t$ of day-2 and -5 precipitation forecasts over 4 different regions selected from Figs. 1 and 2. Over the tropics (30°S–30°N, 0°–360°), the average RMSE$_t$ is about 6.5 mm day^{-1} for day-2 forecasts. For day 5, RMSE$_t$ is higher by about 1 mm day^{-1}. Over South Asia (10°S–30°N, 60°–110°E), the error is substantially higher than the global tropics. The average RMSE$_t$ over this region was about 12.3 and 13.5 mm day^{-1} for day-2 and -5 forecasts, respectively. The error further increases over the Indian region (8°–28°N, 70°–90°E) where average error for day 2 (day 5) was about 15.8 (18.1) mm day^{-1}. The errors are low over North America (0°–30°N, 130°–60°W) compared to those over South Asia or the Indian region. These seasonal mean forecast errors over South Asia are much higher than another version of the ECMWF model that was a part of the Development of a European Multimodel Ensemble System for Seasonal-to-Interannual Prediction (DEMETER) project (Palmer et al. 2004). In Chakraborty and Krishnamurti (2006) it was shown that the average RMS error over the south Asian region from the ECMWF model's seasonal prediction for June–September ranges between 1.5 and 2.0 mm day^{-1} during 1989–2001 (see Fig. 5 of that study). This difference in forecast error could be due to resolution. In the previous study, a 2.5° × 2.5° dataset was used. However, the present study uses 0.25° × 0.25° resolution dataset.

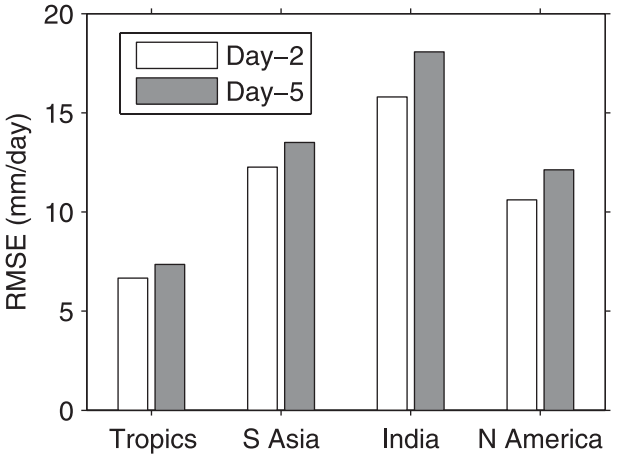

FIG. 3. Mean RMS error of precipitation (mm day^{-1}) for days 2 and 5 over the tropics (30°S–30°N, 0°–360°), South Asia (10°S–30°N, 60°–110°E), Indian region (8°–28°N, 70°–90°E), and North America (0°–30°N, 130°–60°W) during June–September 2008.

However, the variation of forecast error with regions is similar in both the studies.

Figure 4 shows the mean RMSE$_t$ in precipitation forecasts for days 2, 5, and 8 over the tropical land and ocean at different ranges of observed (TRMM) mean and day-to-day variability (standard deviation) of precipitation. At first, RMSE$_t$ of the daily time series of precipitation was calculated at every grid over the tropics for the June–September 2008 season. Similarly, mean and standard deviation at every grid were calculated from the TRMM daily datasets. Now, RMSE$_t$ of forecasted precipitation were averaged for different ranges of observed mean and standard deviation of precipitation. The result is shown in Fig. 4. During day 2, high RMSE$_t$ is seen over places where the observed mean and standard deviation of precipitation is high. This is true both for land and ocean. Over ocean large day-to-day variability in precipitation is noticed even where the observed seasonal mean is low. This is unlike over land where, in general, variability increases with the mean value.

The average RMSE$_t$ increases during day 5 (Figs. 4c,d) of forecasts as compared to day 2 (Figs. 4a,b) in all ranges of observed mean and variability. However, note that over land the increase in RMSE$_t$ is more where day-to-day variability (measured by standard deviation) is large compared to that where seasonal mean is large but variability is low. This is more prominent at longer lead times (day-8 forecasts; Figs. 4e,f). The results were very similar for the South Asian monsoon region. This could be due to the fact that there is no ocean–atmosphere coupling in the model. This issue is further discussed next.

Figure 5 shows the RMSE$_s$ in precipitation forecasts for days 2 through 10 over the tropics (30°S–30°N, 0°–360°) and South Asia (10°S–30°N, 60°–110°E) separately over land and ocean. Note that the increase in RMSE$_s$ from days 2 to 10 is less compared to the error in day 2. This shows that the error growth is quick and that the model reaches its quasi-climatic condition within 12–24 h of integration. Beyond about 36 h of the initial condition, the rate of error growth is minimum compared to what it was up to that time. Figure 5 also indicates that the error in precipitation forecasts is much higher over South Asia as compared to the tropics as a whole. The day-2 RMSE$_s$ for tropical ocean (land) was around 8.5 (9.0) mm day^{-1}. These values were about 12.5 and 16 mm day^{-1}, respectively, for South Asia. Note also that the growth of RMSE$_s$ from day 2 to 10 is larger over the ocean as compared to that over land. This is particularly true for the South Asian oceans where the day-to-day variability of precipitation is high.

b. *Forecasts over the South Asian region*

Monthly and seasonal mean precipitation over the South Asian (10°S–30°N, 60°–110°E) land and ocean for day-2–10 forecasts are shown in Fig. 6 along with the TRMM estimates. Over land (Fig. 6a), large errors in precipitation forecasts is seen as early as during day 2. There is not much variation in the errors (except showing a trend of decrease during August) for day-2–10 forecasts. Notice that the errors are larger during June and July and minimum during September. The seasonal mean [June–September (JJAS)] values show a positive bias in model forecasts of about 2 mm day^{-1} for all lead times.

In contrast to that over land, the bias in ECMWF model forecasts over ocean is lower for shorter lead times during all the months of northern summer (Fig. 6b) for the South Asian region. The model forecasts higher than observed precipitation by about 0.2 mm day^{-1} for day 2 during June and July (and in JJAS mean). This positive bias increases to about 2.5–3.0 mm day^{-1} for day-10 forecasts during June, July, and JJAS mean. The increase in error with lead time is not as large during August and September. These results were similar over tropical land and ocean as well (not shown). That is, the model overestimates precipitation over the entire tropical land and ocean parts. However, unlike that for the ocean parts of the South Asian region, there is no considerable change in bias with lead time when the entire tropics is considered. This is consistent with the decrease in average precipitation bias during August seen in Fig. 6, which was reflected in JJAS mean values as well.

To investigate the cause behind more rapid increase of error over ocean than over land with forecast lead time, we have calculated the RMSE$_s$ and spatial correlation of 2-m air temperature forecasts over the South Asian monsoon region during July 2008 (Fig. 7). The 2-m

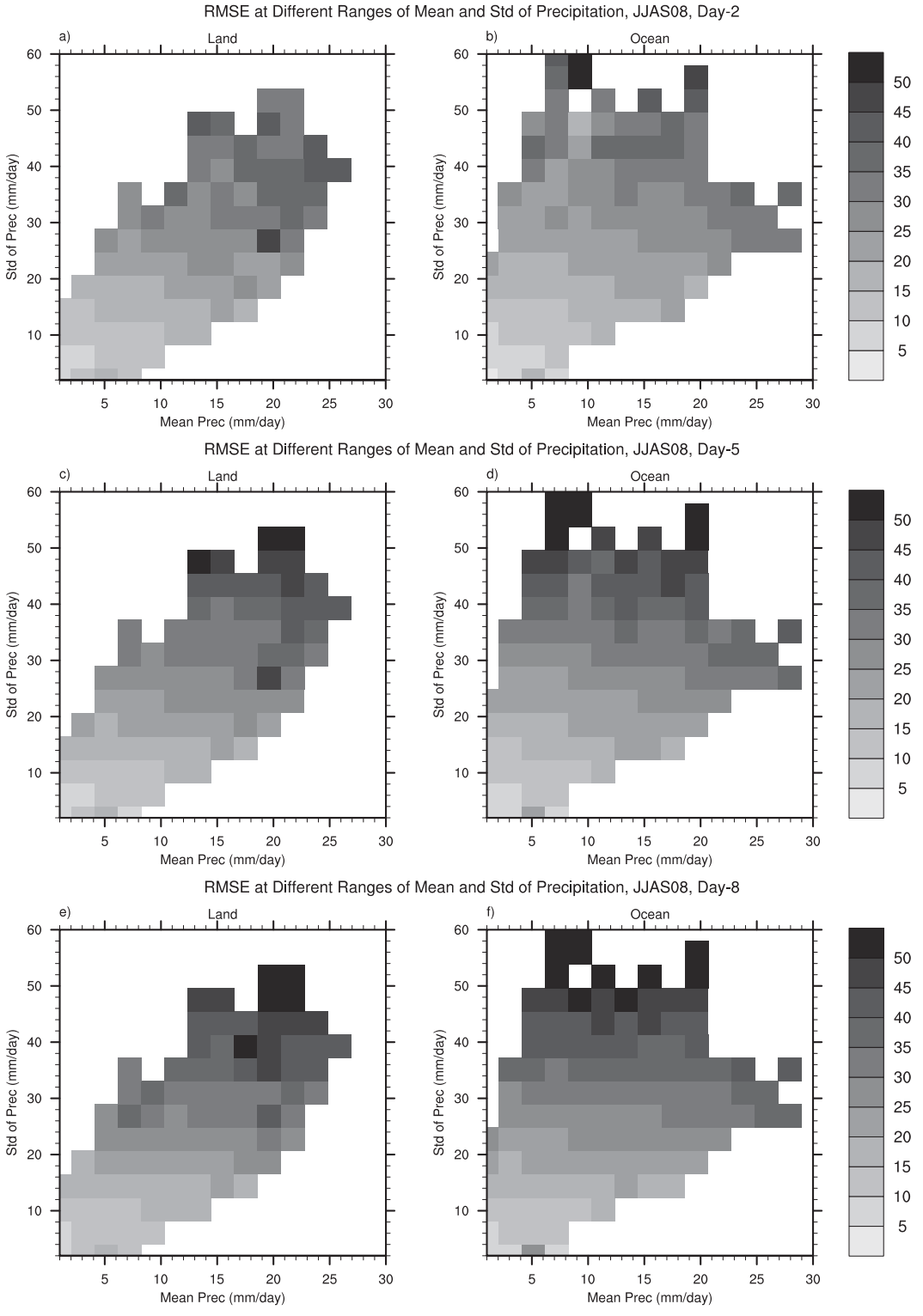

FIG. 4. Average RMS errors in precipitation forecasts for days 2, 5, and 8 over the tropical land and ocean at different ranges of observed mean and variability of precipitation during June–September 2008.

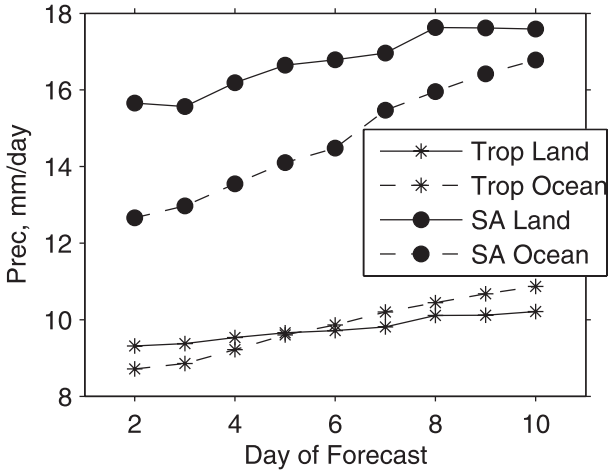

FIG. 5. RMS error of daily precipitation forecasts (mm day^{-1}) for days 2–10 during June–September 2008 over tropical (30°S–30°N, 0°–360°) and South Asian (10°S–30°N, 60°–110°E) land and ocean.

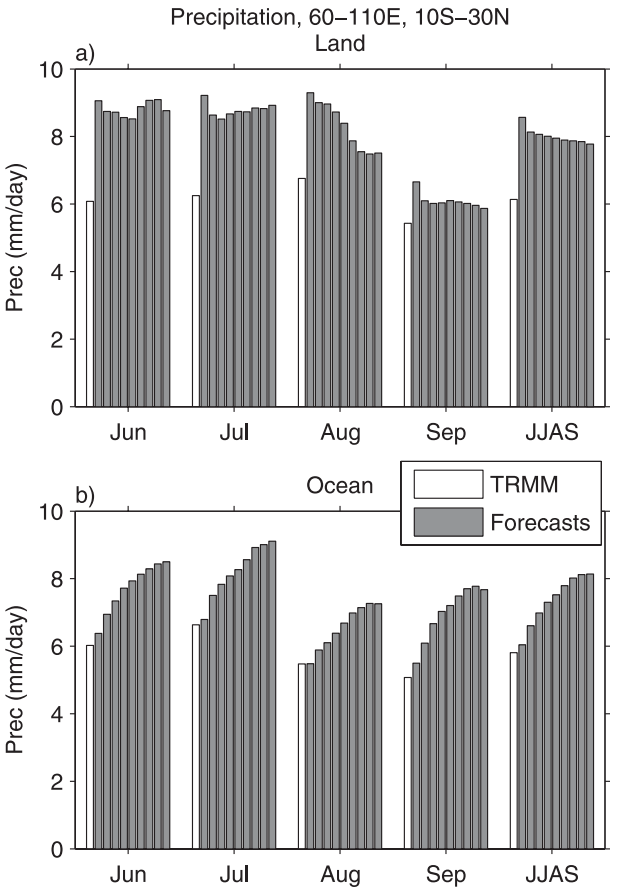

FIG. 6. Mean precipitation over South Asian (10°S–30°N, 60°–110°E) land and ocean from TRMM estimates and model forecasts for days 2–10.

air temperature was chosen because this parameter closely corresponds to the surface temperature. RMSE$_s$ over land (Fig. 7a) from the model forecast is 0.8–1.0 K higher than that over ocean. The rate of increase of RMSE$_s$ with forecast lead time is of the same order over land and ocean parts of the South Asian monsoon region. Hence, the 2-m air temperature error over land remains higher than that over the ocean by almost the same amount up to day-10 forecasts.

Spatial correlation of 2-m air temperature (Fig. 7b), on the other hand, shows a different picture. This figure shows that the spatial correlation over land always remains much higher compared to that over ocean. The rate of decrease of spatial correlation with days of forecasts is small over land. On the other hand, over ocean the spatial correlation drops sharply from day-2 through day-8 forecasts after which it more or less remains constant up to day 10.

The atmospheric GCM for medium-range weather forecasts used in this study had observed values of sea surface temperature (SST), which were prescribed as initial conditions. This cannot take into account the change in SST that will occur due to air–sea interaction. However, the GCM used a land surface model that was totally interactive with the atmospheric component. This allows change in the surface temperature with change in parameters like precipitation, evaporation, winds, and radiative fluxes. Therefore, if the spatial pattern of these parameters is reasonably forecasted by the model, the spatial pattern of the 2-m air temperature will also closely correspond to the observation. However, over the oceans, due to absence of feedback mechanism, the atmospheric parameters cannot change the surface temperature. This leads to a wrong pattern of near-surface air temperature over the oceans as compared to that over land, and the spatial correlation decreases rapidly with forecast lead time. This, in turn, affects the precipitation forecast skills (Figs. 5 and 6).

c. *Northward migration of convection*

Figure 8 shows the time–latitude variation of mean precipitation over 83°–93°E from TRMM estimates and day-2, -5, and -8 forecasts. Three major phases of northward movement of convection zone from near the equator to about 25°N are noticed in Fig. 8a during this season (middle of June, end of July, and middle of September). These phases are marked by ellipses on the figure. The model was able to forecast the first and third phase of northward propagation during day 2. The second phase of propagation during the end of July was marked by a deep convective zone at around 15°N in the model forecasts. This was very similar to that observed in the TRMM estimates. One noted problem of the model is to

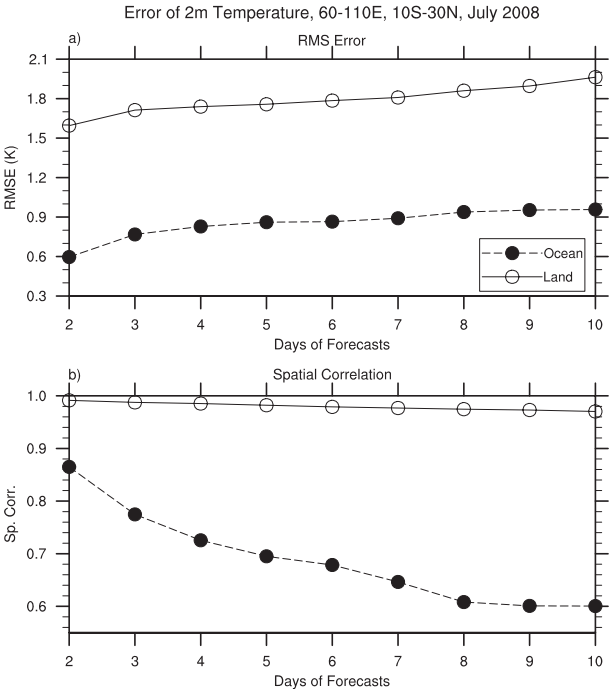

FIG. 7. Error in air temperature at 2 m height for days 2–10 of forecasts during July 2008 over the South Asian land and ocean: (a) RMS error and (b) spatial correlation.

forecast higher value of low intensity precipitation than the observed, especially during June–August. This error decreased during September.

The forecast skill of the model decreases during days 5 and 8 (Figs. 8c,d). The first and last phases of northward propagation of precipitation zone were reasonably captured during day-5 forecasts. However, the northward propagation was completely unorganized in day-8 forecasts. Moreover, the model shows large frequency of low intensity precipitation during days 5 and 8 as compared to the TRMM estimates. The pattern correlation (PC) of the forecast fields with the observation decreases during day 5 (0.44) and 8 (0.33) as compared to that during day 2 (0.63).

The loss of coherent phase at longer lead-time forecasts for the northward propagation of precipitation could be a consequence of degraded forecasting skill at every geographical location at these lead times. For a propagating system, this degraded skill can arise from two reasons. At first, the model may not be able to generate a convective system (genesis) that is not present in the initial data or in the previous time step. Or, a system that is present in the model may not be propagating realistically because of an error in the model or in the surface boundary conditions used over ocean. The exact reason behind the loss of coherent phase at longer lead time needs further detailed studies.

d. Equitable threat score

Equitable threat score (ETS) of daily precipitation forecasts over the South Asian land and ocean for different thresholds are shown in Fig. 9. ETS is defined as

$$\mathrm{ETS} = \frac{H - E}{F + O - H - E}, \tag{3}$$

where F and O are, respectively, the number of grids over which forecast and observed precipitation exceed a specified threshold, H is the number of grids that correctly forecast more than the specified threshold (also termed as "hit"); $E = F \times O/T$, T being the total number of grids over the region. ETS can vary between $-1/3$ and 1. A higher score signifies a better forecast.

Figure 9a shows that ETS of precipitation forecasts over South Asian land reaches highest value (~0.6) at threshold 0.1 mm day^{-1} for day-2 forecast. The ETS decreases for thresholds higher or lower than 0.1 mm day^{-1}. This shows that the ECMWF model has difficulty in forecasting precipitation values close to zero. Similarly, for thresholds higher than 2 mm day^{-1}, ETS decreases sharply and reaches a value of about 0.1 for thresholds at 30 mm day^{-1}. Therefore, the model performs poorly for extreme values of precipitation. Figure 9a also shows that ETS for a single threshold decreases with longer lead time. However, this change is not as large as it is for changing precipitation threshold.

Over ocean (Fig. 9b), the higher ETS is seen for threshold of 2 mm day^{-1} for day-2 forecasts. ETS values decreases slowly at thresholds lower than 2 mm day^{-1}. However, for thresholds greater than 2 mm day^{-1}, ETS decreases sharply and reaches a value of about 0.15 for threshold 35 mm day^{-1}. Comparing Figs. 9a,b, we find that for a single threshold ETS over land is higher than that for the ocean. Moreover, the rate of decrease in forecast skill score with lead time is higher over ocean than that for land.

To understand the bias in precipitation forecast of the model, we have plotted the bias score over South Asian land and ocean in Fig. 10. Bias score is defined as

$$\mathrm{BIAS} = \frac{F}{O}, \tag{4}$$

where F and O are total number of forecast and observed grids above a threshold, respectively. The value of bias score can vary from 0 to positive infinity and a value of 1 signifies that the number of grids above a particular threshold in the observation and forecast fields are the same. Figure 10a shows that ECMWF model generally tends to overestimate precipitation up to a threshold of about 30 mm day^{-1} for day-2 forecasts.

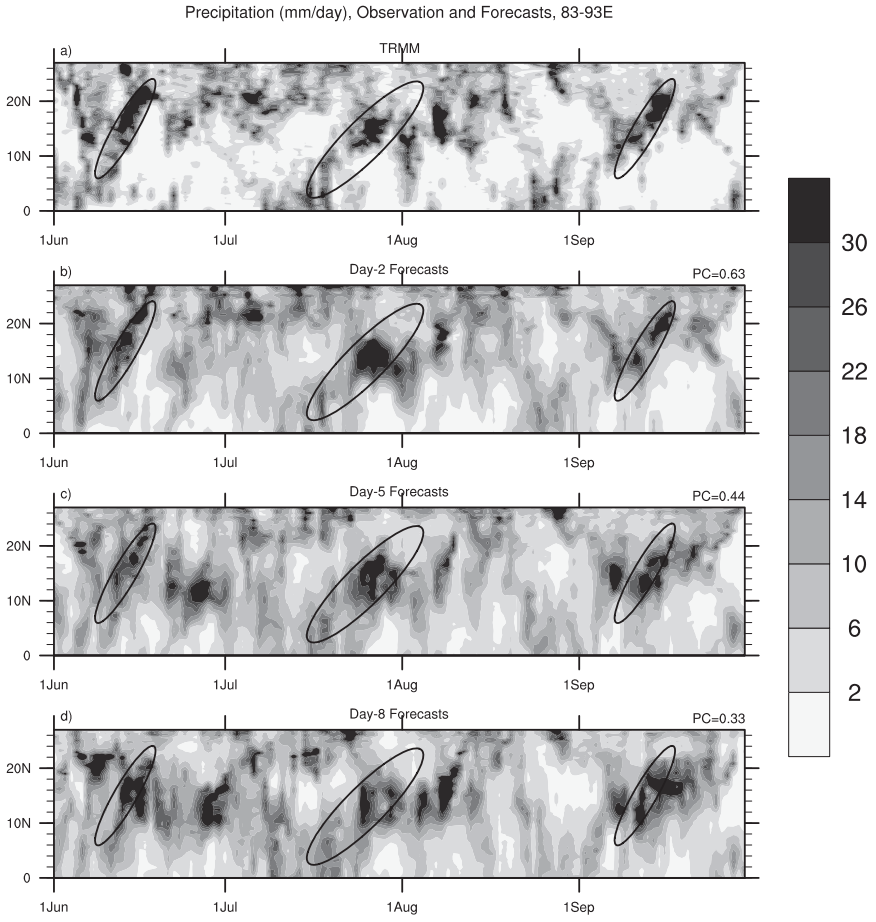

FIG. 8. Precipitation as a function of time and latitude averaged over 83°–93°E from (a) TRMM estimates and model forecasts during days (b) 2, (c) 5, and (d) 8. The pattern correlations of the forecast fields with the observed fields are indicated as numbers at the top-right corner of the (b)–(d).

For thresholds up to 2 mm day^{-1}, bias scores of day-2 forecasts were better (closer to 1) than that of days 5 and 8. However, for thresholds 4–25 mm day^{-1}, day-5 and -8 forecasts perform better than day 2 in terms of bias score over South Asian land.

Over the oceanic part of the same region (Fig. 10b), bias scores are usually farther away from 1 than that over land at smaller thresholds. However, for moderate thresholds (2–15 mm day^{-1}), the model performs better over ocean than over land. Moreover, ECMWF model underestimates high precipitation (>25 mm day^{-1}) over ocean. A comparison of Figs. 10a,b also shows that the reduction in forecast skill at a longer lead time is higher over the ocean than that over land. Note that, over land, the bias is smaller (closer to 1) for longer lead times for thresholds higher than 4 mm day^{-1}. This means that, over this region, less number of grids exceed the threshold than observed number of grids.

The false alarm ratio (FAR) of precipitation forecasts, which is defined as

$$\mathrm{FAR} = \frac{F - H}{F}, \tag{5}$$

where the symbols are same as those used in Eq. (3), measures the fraction of grids over which the forecast of an event was wrong to the total number of grids over which that same event was forecast. A value of 0 for this parameter signifies a perfect forecast and 1 signifies completely wrong forecast. Figure 11 shows that, both over land and ocean, FAR has lower value for day-2 forecasts than that of days 5 and 8. Moreover, similar to that of ETS, the forecast skills in terms of FAR is best at thresholds 0.1 mm day^{-1} over land and 2 mm day^{-1} over ocean. The rate of increase in FAR for higher thresholds is large over land than that for ocean. This

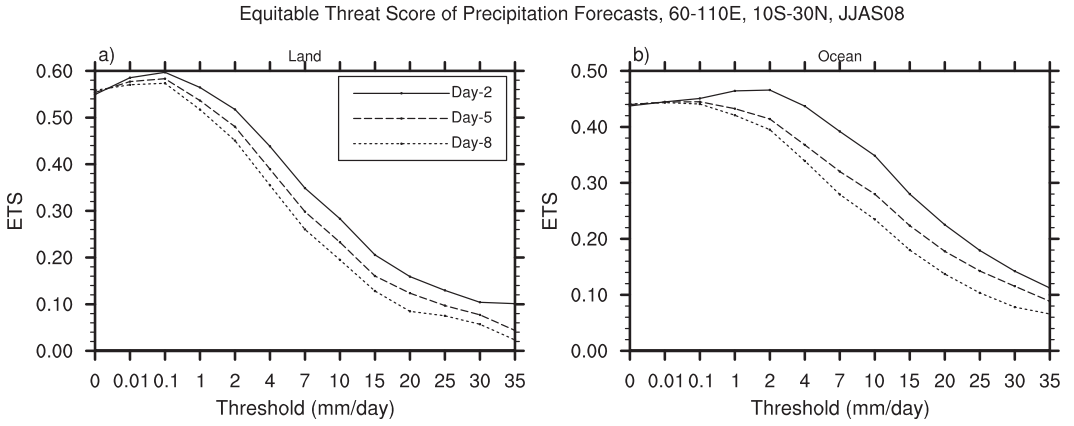

FIG. 9. ETS of precipitation forecasts during days 2, 5, and 8 over the South Asian (10°S–30°N, 60°–110°E) land and ocean at different thresholds.

shows that over land, the number of false prediction of heavy precipitation events is large. Figures 11a,b also show that the decrease in forecast skill at larger lead time is more over the ocean than that over land. This is consistent with that seen for RMS errors (Figs. 4 and 5), mean precipitation (Fig. 6), equitable threat score (Fig. 9), and bias score (Fig. 10). All these results suggest a possible error in SST forcing and coupling at longer lead time given to this weather forecast model. It is also possible that these errors arise due to the drift in the model toward its climatic conditions. This needs to be investigated further using sensitivity experiments, which require a separate study.

e. Frequency distribution of precipitation

Relative occurrences of daily precipitation intensity during June–September 2008 at different intervals over the South Asian land and ocean is shown in Fig. 12 from TRMM estimates, and day-2, -5, and -8 forecasts. The interval that is defined from 0.0 to 0.001 mm day^{-1} can be considered as *no-precipitation* or *zero-precipitation* considering precision errors in the digital data. The basic characteristics of the frequency distributions did not change while changing the upper limit of this interval to 0.0001 or 0.01 mm day^{-1}. TRMM estimates show that for about 45% cases over land and about 55% cases over ocean there was no precipitation during a day. The frequency of observed (TRMM) precipitation decreases with higher intensity both over land and ocean. The model forecasts show large errors in the frequency distribution of precipitation. The frequency of zero precipitation is only about 5% over land and 1% over ocean in the model forecasts. On the other hand, frequency of low intensity precipitation (0.001–5.0 mm day^{-1}) is much higher in the model forecasts, the error being larger over the ocean than over land. For moderate to heavy precipitation (5–10, 10–20, and 20–40 mm day^{-1}), the forecasted precipitation frequency shows the same

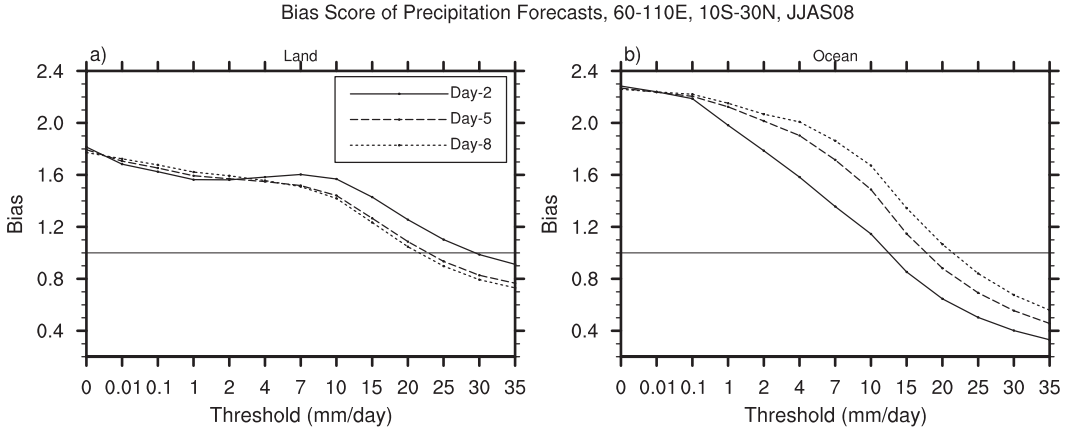

FIG. 10. Bias score of precipitation forecasts during days 2, 5, and 8 over the South Asian (10°S–30°N, 60°–110°E) land and ocean at different thresholds.

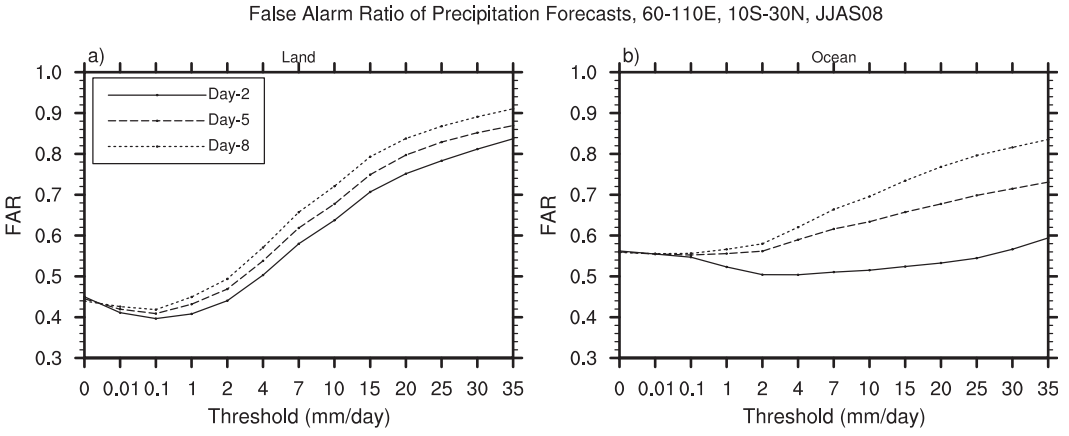

FIG. 11. False alarm ratio of precipitation forecasts during days 2, 5, and 8 over the South Asian (10°S–30°N, 60°–110°E) land and ocean at different thresholds.

decreasing trend as that in the TRMM estimates. However, the model generally underestimates very heavy precipitation at (40–80 mm day^{-1}), especially over the South Asian oceans. This is true for day-2, -5, and -8 forecasts. However, note that the increase in error from day-2 to day-5 and -8 forecasts for precipitation intervals of 5–40 mm day^{-1} is higher over the ocean than that over land. This is consistent with the results presented in previous sections that the increase in error with lead time is higher over the ocean than that over land.

f. Forecast skill as a function of dimension of the region

Often the spatial and temporal phase errors in the model forecasts can be reduced by averaging over a larger region. Thus, a model can show poor skill over a smaller domain but high skill when averaged over a larger region. To investigate the skill of precipitation forecasts by the ECMWF model as a function of domain size, we have chosen many different dimensions of averaging between 8°–28°N and 70°–90°E, starting at the middle of the region (shown by a dot in Fig. 13). The temporal correlation was chosen as the skill metric here to measure the day-to-day variability in the model compared to the observation. It is possible that even when the day-to-day variability is correct, the values could be very wrong. However, it was seen that (not shown) there was no large constant bias in the model in these lead times that can result in a consistent high value in RMS error. Figure 14 shows that, in general the skill of forecasts is higher when the lead time is shorter and the area dimension is larger. The increase in forecast skill is much higher with the dimension of averaging for days 2 and 5 up to about 5°. After that, an increase in the averaging dimension does not significantly improve the short-range (days 2 and 5) forecast skills. On the other hand, the rate of increase in forecast skills is much slower for days 8 and 10, and this rate remains almost constant throughout the dimension range.

Figure 15 shows the temporal correlation of precipitation forecasts averaged over four different domains (shown by the boxes in Fig. 13) as a function of the lead time. Over the smallest sized domain (0.25° × 0.25°), the rate of decrease in forecast skill with lead time is highest, and attains a near steady value after day 5. The forecast skill increases with the domain size at a given lead time. Moreover, the rate of decrease in skill

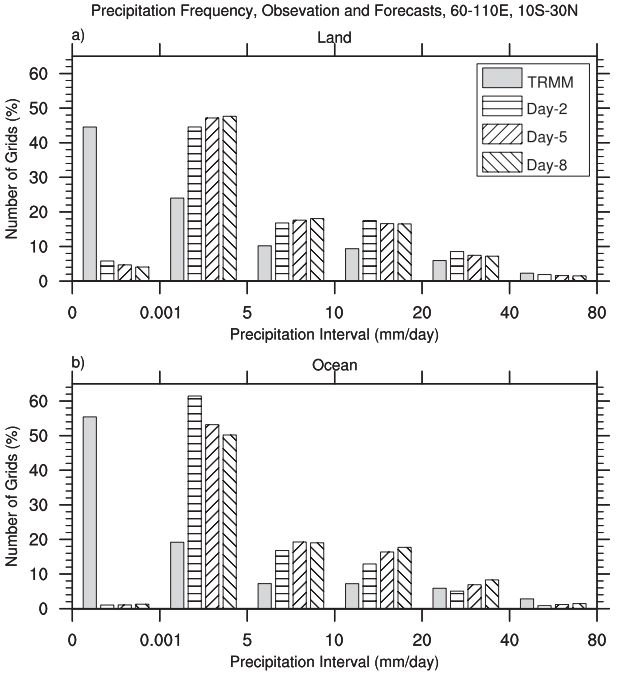

FIG. 12. Frequency of observed and forecast precipitation at different intervals over the South Asian land and ocean.

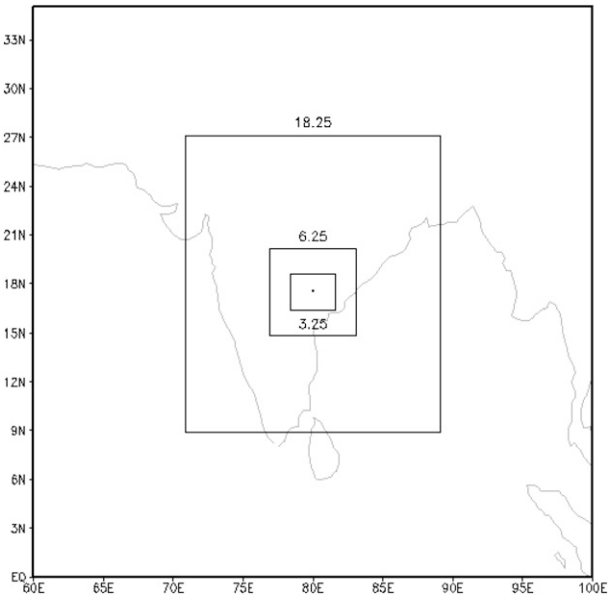

FIG. 13. Regions of spatial average for Figs. 14 and 15.

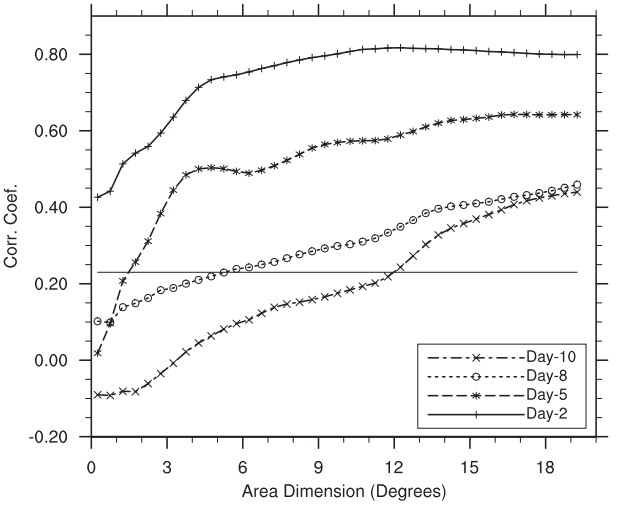

FIG. 14. Time correlation of daily precipitation forecasts vs spatial scale at different lead times of 2, 5, 8, and 10 days over the Indian region.

with lead time is least for the 18.25° × 18.25° domain, over which the spatial correlation attains a steady value after day-8 forecasts.

The results presented here do not depend on the center location chosen. It was seen that (not shown) if the center location is (25°N, 80°E), instead of the present (18°N, 80°E), the nature of the skill score curves presented in Figs. 14 and 15 essentially remains similar.

These results show that it is possible to significantly improve the model forecast skill with increase in the domain size of averaging. However, for short-range forecasts (lead time of 2–5 days) the skill does not improve significantly beyond a region of about 5° × 5° in dimension. However, for longer lead times (6–10 days), a larger domain of average can significantly improve the skill of precipitation forecast over the Indian monsoon region.

g. Diurnal cycle of precipitation

Convection has a large amplitude of variation in the diurnal time scale. Usually, this diurnal variation is higher over land than that over oceans because of the large heat capacity of the seawater. Several previous studies have demonstrated the importance of an accurate prediction of diurnal cycle on various weather and climate parameters (Bergman and Salby 1997; Dai and Deser 1999; Dai 2001; Slingo et al. 2003; Trenberth et al. 2003; Chakraborty et al. 2007). Using observed winds and precipitation datasets, Krishnamurti and Kishtawal (2000) have shown that divergent circulations of the Asian summer monsoon have a continental-scale diurnal mode. Chakraborty and Krishnamurti (2008) have shown that this continental-scale diurnal mode contributes to about 10% of the total energy of the monsoon circulation. Therefore, it is important to examine the skill of the ECMWF model in forecasting the diurnal cycle of convection over the Indian monsoon region.

Figure 16 shows the total precipitation at every 3-h interval of a day averaged during 1–31 July 2008 as obtained from TRMM estimates. This figure shows that the foothills of the Himalayas and the oceans received active convection during late night and morning hours (0000–1200 LST). Convection was active over land during the afternoon and evening hours (1500–2100 LST).

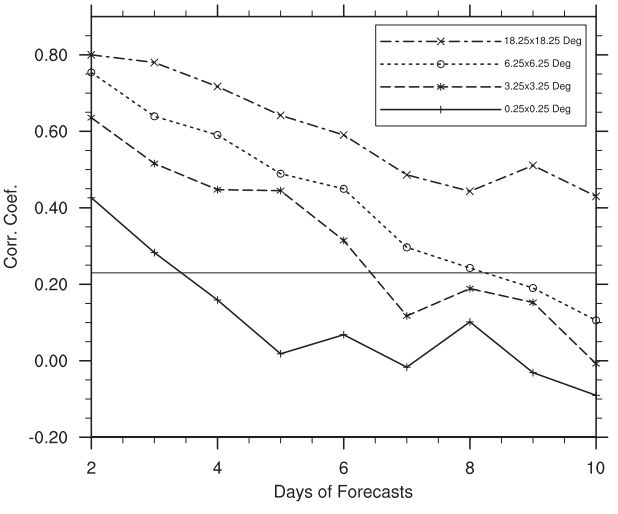

FIG. 15. Time correlation of daily precipitation forecasts vs lead time at different spatial scales over the Indian region.

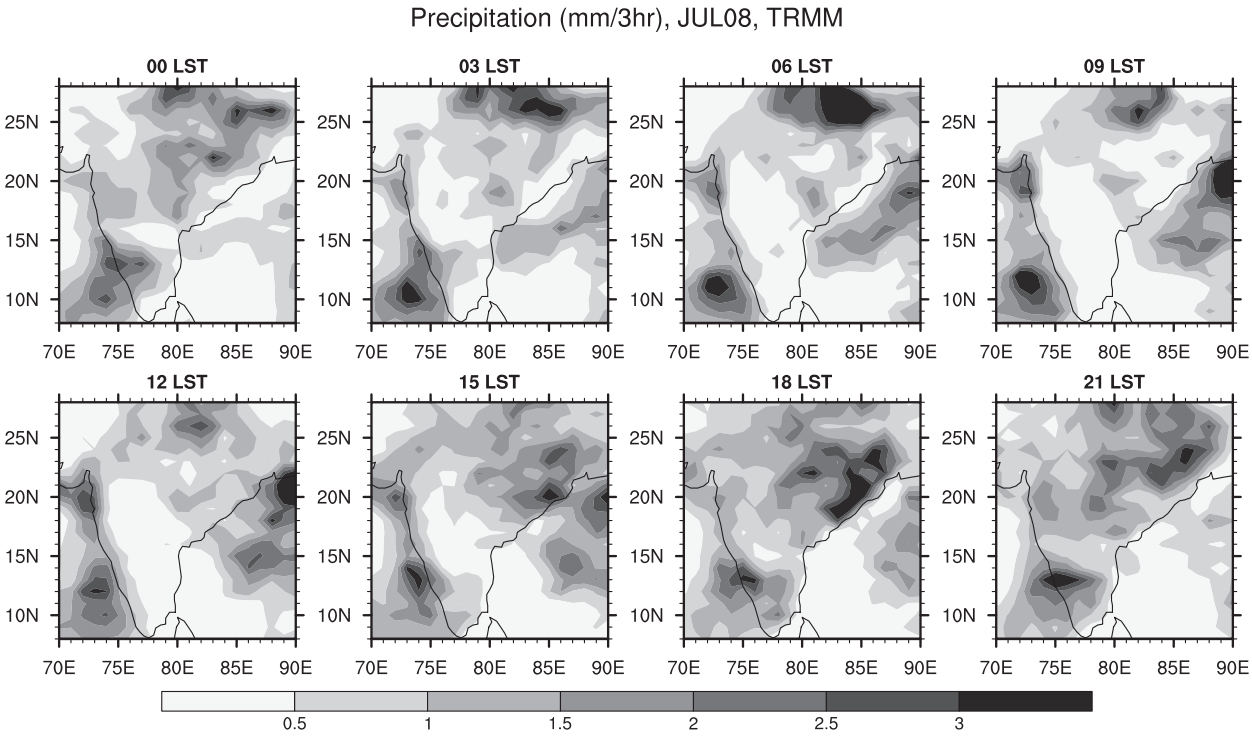

FIG. 16. Monthly mean 3-hourly precipitation during July 2008 from TRMM satellite estimates.

Although an afternoon maximum over land and a morning maximum over ocean is the general characteristics of the phase of diurnal cycle of the convection (e.g., Dai 2001), many studies show a regional dependency of the phase both over land and oceans (e.g., Shin et al. 1990; Janowiak et al. 2005; Wallace 1975; Dai et al. 1999; Yang and Slingo 2001; Yang and Smith 2006; Krishnamurti et al. 2007; Chakraborty et al. 2007). However, here we will consider the overall phase of the diurnal cycle over the Indian monsoon region.

Figure 17 shows the spatial variation of error in model-predicted 3-hourly precipitation during July 2008 for day-4 forecasts. This figure shows that over land, the model overestimates precipitation during the morning hours (0900–1200 LST) and underestimates it during the afternoon to evening hours (1800–2100 LST). On the other hand, over the oceans the model largely overestimates precipitation during the evening to morning hours (2100 and 0000–0900 LST). Another interesting point is that the model underestimates precipitation over the northern Bay of Bengal during the morning hours when the observed diurnal cycle attains a peak over this region (Figs. 16 and 17). This signifies that the model missed the phase of the diurnal cycle of precipitation. RMSE_s (spatial correlations) of 3-hourly forecasts (indicated at the top of each panel) varies from 0.8 to 1.2 mm $(3\ \mathrm{h})^{-1}$ (0.12–0.38). Figure 17 also shows that these errors get reduced significantly when the data is averaged over a day (errors of daily averaged data are indicated below the title).

To examine the phase of diurnal cycle of precipitation in observation and model forecasts, 3-hourly precipitation at 8 time points of a day averaged during June, July, August, and September of 2008 from TRMM and day 4 of the model forecasts over the Indian monsoon region (8°–24°N, 70°–90°E) are shown in Fig. 18. We have restricted the northward bound of the region to 24°N to exclude the Himalayan foothills, which shows a very different phase of diurnal cycle compared to rest of the Indian region. Over land, the TRMM data show a peak in precipitation at 1800–2100 LST. The model forecasts show the peak at 1200 LST, indicating a phase error of about 6 h. Note also that the amplitude of the diurnal cycle over land was underestimated by the model during June and overestimated during August. Over the oceans, the observed data shows a peak in precipitation at around 0900–1200 LST. However, the day-4 forecasts of the model show a peak at the midnight to early morning hours (0000–0300 LST). Therefore, the model has a phase error of about 9–12 h over the oceans. Moreover, the amplitude of the diurnal cycle is much higher in the model forecasts as compared to the TRMM estimates. Note that the amplitude errors over land were not as high as that over the oceans.

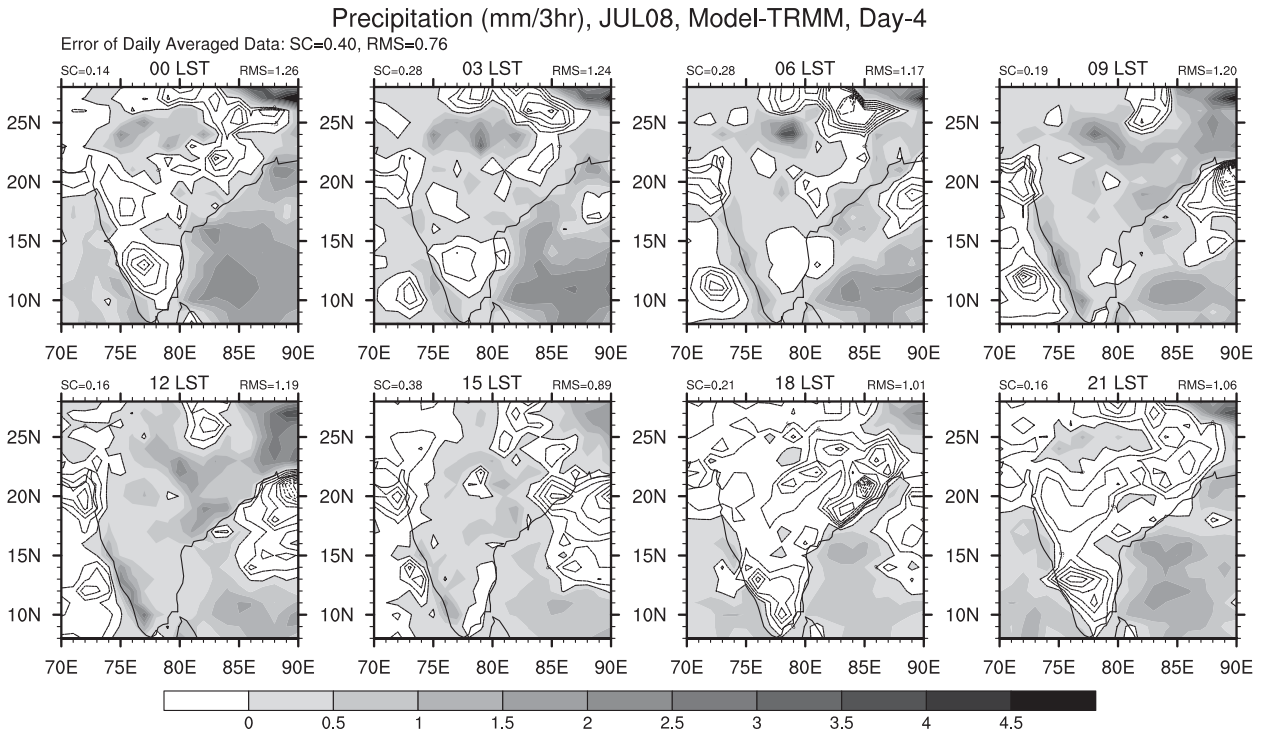

FIG. 17. Monthly mean difference of 3-hourly precipitation between TRMM satellite estimates and ECMWF model forecasts during July 2008. The 3-hourly spatial correlations and RMS errors between the observation and model are indicated. The corresponding error statistics for the daily mean data is shown at the top-left corner. Positive values of the differences are shaded and negative values are contoured. Contour interval is 0.5 mm $(3\ \text{h})^{-1}$.

The evolution of the diurnal cycle as a function of forecast lead time in the model is examined in Fig. 19. Time series of 96-h-long 3-hourly precipitation starting at 1500 UTC 2 July 2008 averaged over the Indian region (8°–28°N, 70°–90°E, land and ocean separately) derived from TRMM and model forecasts were considered to create this figure. For the model, this corresponds to the initial condition of 1200 UTC 2 July 2008. The entire forecast period up to 96 h was divided into four 24-h periods of different lead times. Diurnal cycle of precipitation from the 8 time points of a 24-h period was constructed by taking the first harmonic of fast Fourier transformation of the time series. This methodology is similar to that was used in extracting diurnal time period in Chakraborty et al. (2007). We have plotted only up to 96 h of forecasts since the YOTC provides 3-hourly datasets only up to this time. The subsequent outputs are 6 h apart and are not very useful to study diurnal cycle. Figure 19 shows that over land, the TRMM estimates have a peak of diurnal cycle during afternoon to evening hours in all 4 days. The model shows a peak at 1500 LST during 0–24-h forecasts. This corresponds to an error of about 3 h in the phase of the diurnal cycle. However, during 24–48 h, the phase of diurnal cycle the model shifts to 1200 LST, 9 h early compared to the TRMM phase. During the following forecast hours, the peak precipitation from the model varies between 0900 and 1500 LST and the error in phase varies between 9 and 12 h. Over the ocean part (Fig. 19, bottom panels), TRMM data shows the peak of diurnal cycle between 0900 and 1200 LST. The model shows the phase of diurnal cycle at 1200 LST during 0–24 h of forecasts (phase error of about 3 h). The phase error of the model is small during 24–48-h forecasts as well. However, the error in phase increases for the following hours of forecasts when the model shows the early morning maximum but the TRMM estimates show the noon maximum.

Therefore, this shows that the error in the diurnal cycle is at a minimum during the first 24 h of forecasts. The error increases during the subsequent forecast hours and remains almost constant up to the 96-h forecasts.

h. Forecasting of monsoon system

This section illustrates the skill of the ECMWF model to forecast a monsoon low pressure system that appeared during the middle of June 2008 over Bay of Bengal (BoB). On 12 June, the system was unorganized and situated over central BoB in the TRMM dataset (Fig. 20a). The day-2 forecast of the model (Fig. 20b) also shows an unorganized system covering the entire

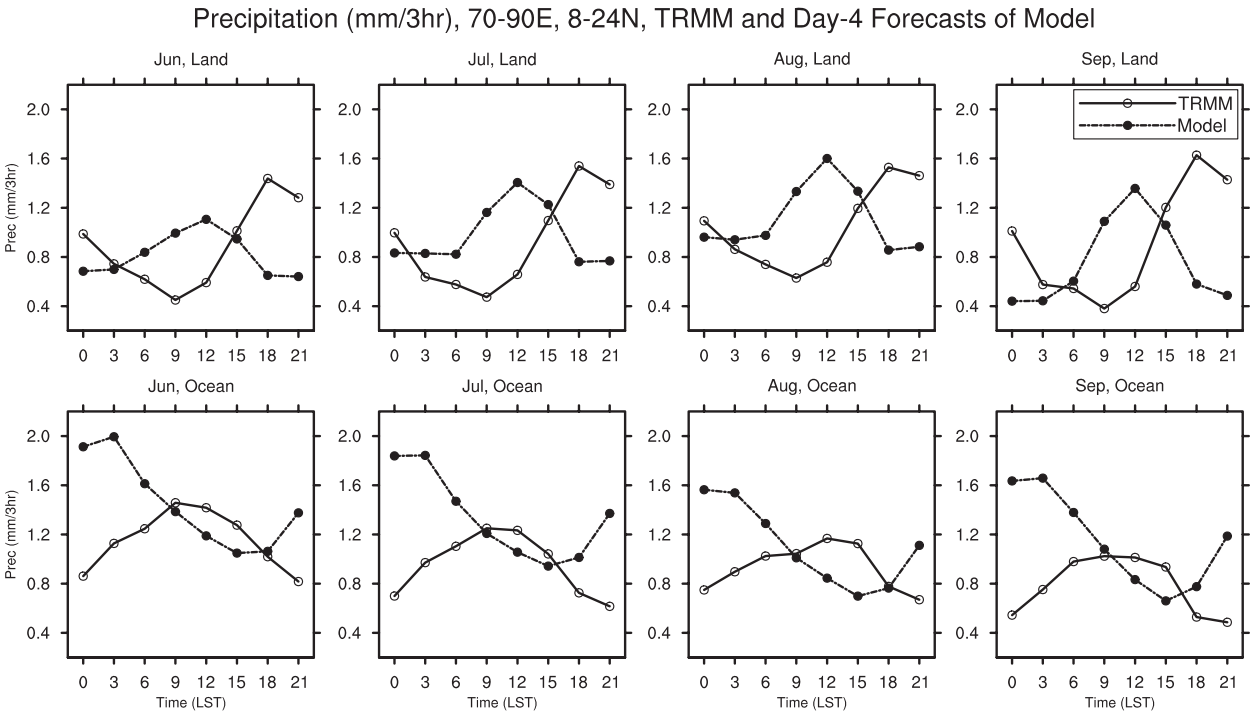

FIG. 18. Diurnal cycle of precipitation over 8°–24°N, 70°–90°E (land and ocean) obtained from TRMM satellite estimates and day-4 forecasts of ECMWF model during June–September 2008.

BoB. However, the model shows more convection over northwest part of the Bay. The day-7 forecast of the model (Fig. 20c) shows an unorganized system from southwest to northeast over the Bay. The $RMSE_s$ and spatial correlation for day-2 (day 7) forecasts were 19.5 mm day^{-1} and 0.22 (20.4 and 0.20) mm day^{-1}. On 14 June, the system became well developed and was concentrated over the north BoB in the TRMM observation (Fig. 20d). The day-2 forecast of the model (Fig. 20e) shows a concentrated system roughly at the same place that in the TRMM datasets. Day-7 forecasts (Fig. 20f) shows a smaller system over northwest BoB. But north–south-oriented precipitation near the Burmese Mountains over the eastern BoB is not very realistic in this forecast. Moreover, higher-than-observed precipitation over the southern parts of BoB during both day-2 and -7 forecasts are unrealistic in the model. Overall, the spatial pattern for day-2 forecasts (SC = 0.58) was better than the day-7 forecasts (SC = 0.12). On 16 June, the system had moved farther northwest and became smaller (Fig. 20g). The day-2 forecast of the model shows a concentrated precipitating zone roughly at the same location over the head of BoB (Fig. 20h). In the day-7 forecast (Fig. 20i), the system is farther south compared to the TRMM estimates. However, the heavy precipitation over the eastern parts of BoB forecasted by the model was not present in the TRMM datasets. The day-2 forecasts showed higher skills (SC = 0.59, $RMSE_s$ = 19.3 mm day^{-1}) compared to day-7 forecasts (SC = 0.13, $RMSE_s$ = 30.9 mm day^{-1}). By 18 June, the system became small and moved entirely over land in the TRMM estimates (Fig. 20j). This is not shown either in day-2 or -7 forecasts (Figs. 20k,l). Moreover, the high precipitation over central-east BoB in day-7 forecasts was completely absent in the TRMM estimates.

This shows that the ECMWF model has reasonable skill in forecasting a propagating monsoon system over the Bay of Bengal during up to at least 48 h in advance (day 2). However, the skill of the forecasts becomes poor during day 7 when spurious precipitation near orography is evident in the model forecasts.

5. Conclusions

The Year of Tropical Convection (YOTC) program, a coordinated observation, modeling, and forecasting initiative by the WCRP and WWRP/THORPEX provides an opportunity to study the multiscale characteristics and interaction of tropical convection with high spatial and temporal resolution datasets. During the YOTC period, the ECMWF model forecasts are available at high resolution up to 10 days starting at 1200 UTC of every day since 1 May 2008. This study utilizes this datasets along with the 3-hourly precipitation obtained

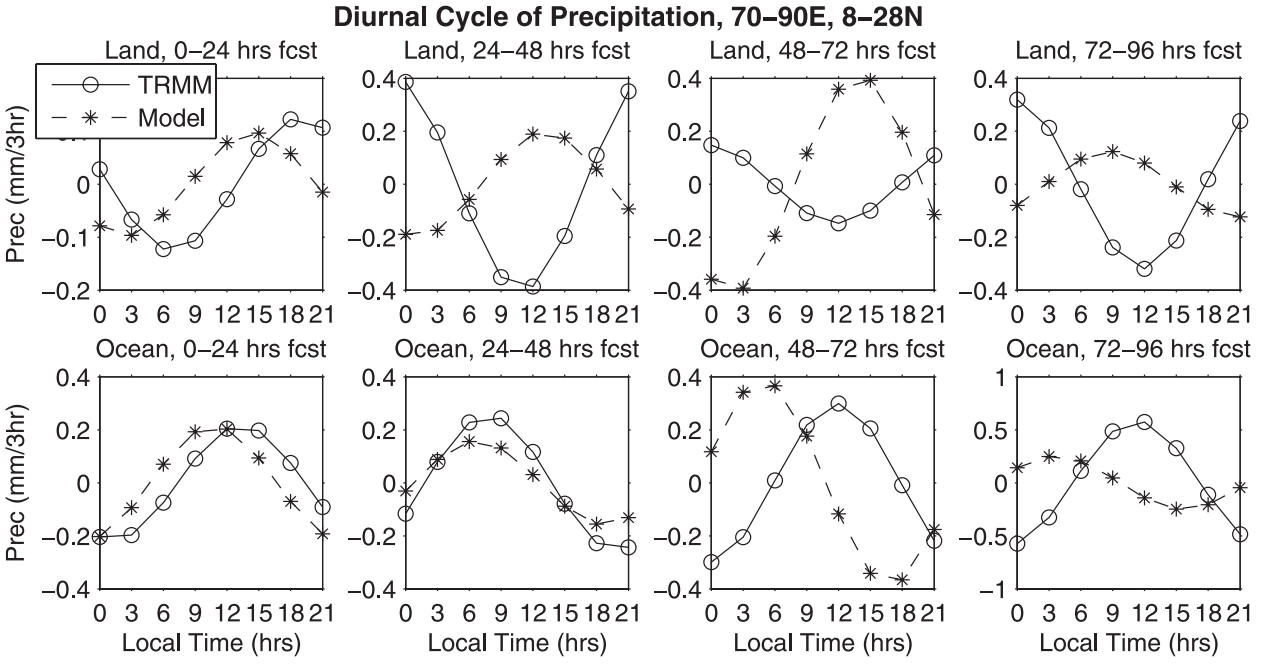

FIG. 19. Diurnal cycle of precipitation over the Indian monsoon region (land and ocean) obtained from TRMM satellite estimates and 0–24-, 24–48-, 48–72-, and 72–96-h forecasts of ECMWF model starting at 1200 UTC 2 Jul 2008.

from TRMM 3B42 product to access the precipitation skill of the ECMWF model over the South Asian monsoon region during June to September 2008.

Our results show that the ECMWF model is able to capture the overall pattern of precipitation up to at least 5-days in advance when daily forecasts are averaged over a season (June–September 2008). However, large error was seen in precipitation forecasts when daily data of the model was compared with that of the TRMM estimates. Over land, the RMS error is large where mean and day-to-day variability of observed precipitation is large. The increase in RMS error with a lead time over land is also primarily confined to these regions. However, over the oceans at a short lead time (day-2 forecasts), the largest errors are obtained where observed data shows high day-to-day variability but moderate amounts of precipitation as well as over the regions with high amounts of precipitation and moderate day-to-day variability. On the contrary to that over land, the RMS error increased most rapidly with lead time where the day-to-day variability in observed data is highest in the oceanic regions. This may be due to a lack of the air–sea feedback mechanism in the model. This could also be due to the natural drift of the model toward its climatic sate. Further investigation is required to obtain a firm conclusion on this.

Furthermore, it was shown that the rate of increase in precipitation forecast error with lead time is higher over ocean than over land. The mean precipitation over the South Asian (10°S–30°N, 60°–110°E) land was overestimated by the model even during day-2 forecasts. The model did not show a large bias in mean precipitation over oceans with short lead times. However, the monthly mean precipitation over the oceans increases rapidly with lead time and by day 8 the error reaches the same order as that over land. It was seen that the rapid increase in precipitation forecast error over the oceans is related to decrease in the forecasting skill of the near-surface air temperature. The absence of air–sea feedback in the atmospheric model cannot change SST according to the atmospheric conditions, which result in a poor skill in forecasting the spatial pattern of near-surface temperature. Over land, because of the presence of interactive land surface scheme in the model, the temperature changes according to the atmospheric conditions and a better forecast of the atmospheric parameters closely correspond to a better forecast of the spatial pattern of the surface and, hence, near-surface air temperatures.

This study also shows the ECMWF model was able to reasonably capture the northward migration of convection zones over the Bay of Bengal up to 5 days in advance.

Study of equitable threat scores, false alarm ratio, and frequency distribution at various thresholds shows that the model had considerable difficulties in capturing near-zero and very heavy precipitation. The model has too few grids with "zero" precipitation as compared to the TRMM estimates. On the other hand, frequency of drizzles

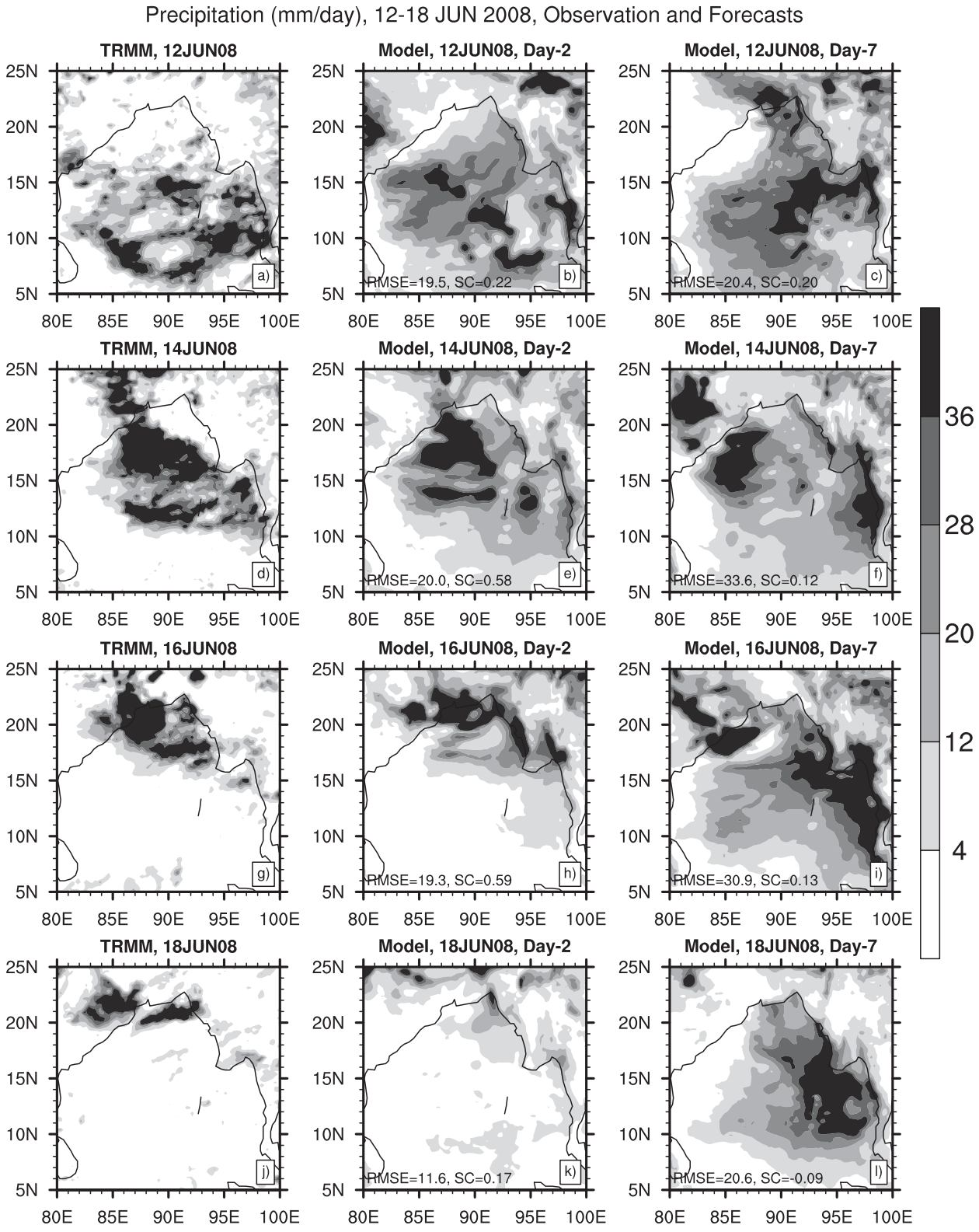

FIG. 20. (a)–(l) Precipitation (mm day^{-1}) from a low pressure system over the Bay of Bengal during 12–18 Jun 2008 as was estimated by TRMM and predicted by the ECMWF model during day-2 and -7 forecasts. The RMS errors (RMSE) and spatial correlations (SC) of the forecasted fields compared to the TRMM data are indicated in (b),(c),(e),(f),(h),(i),(k), and (l).

in the model is much higher than the observed datasets. Frequency of heavy precipitation (>40 mm day^{-1}) was also underestimated by the model.

It was seen that large phase error precipitation forecasts in time and space can be reduced if daily data is averaged over larger spatial domains. However, for short-range forecasts (2–5 days in advance), no gain in precipitation forecast skills is obtained when the region of average exceeds about 5°. For longer ranges (8–10 days in advance), the temporal correlations between the observed and forecasted datasets can be increased significantly by increasing the dimension of the region.

The study of the diurnal cycle using 3-hourly data up to day-4 forecasts show that the ECMWF model has phase error of about 6 h over land and 9–12 h over the oceans. Moreover, the amplitude of the diurnal cycle is very high in the forecasted datasets especially over the oceans. This shift in model forecasted phase results in large error with 3-hourly precipitation [0.5–1.0 mm (3 h)$^{-1}$ or 4–8 mm day^{-1}] both over land and the oceans, which is much larger than the error in daily averaged forecasts. The RMS error in the monthly mean 3-hourly forecasted datasets over the Indian monsoon region varies from 0.80 to 1.2 mm (3 h)$^{-1}$. It has been shown that this error can be significantly reduced if the data is averaged over a day.

This paper demonstrates that the medium-range weather forecast model of ECMWF has a reasonably good forecast skill of precipitation over the South Asian monsoon region up to about 5 days in advance. However, the forecast errors increase rapidly with lead time over oceans possibly due to lack of air–sea interaction in the atmosphere-only GCM. The diurnal cycle of precipitation was seen as a major source of error in this model. A future study will try to investigate the reasons behind this large phase and amplitude error in diurnal cycle in precipitation over the South Asian monsoon region.

Acknowledgments. The forecast datasets used in this study were provided by ECMWF through the YOTC program. TRMM 3B42 datasets were obtained from the NASA GSFC Web site.

REFERENCES

Anthes, R. A., 1983: Regional models of the atmosphere in middle latitudes. *Mon. Wea. Rev.,* **111,** 1306–1330.

Bengtsson, L., and A. J. Simmons, 1983: Medium range weather prediction: Operational experience at ECMWF. *Large Scale Dynamical Process in the Atmosphere,* B. J. Hoskins and R. D. Pearce, Eds., Academic Press, 337–363.

Bergman, J. W., 1997: A numerical investigation of cloud diurnal variations. *J. Climate,* **10,** 2330–2350.

——, and M. L. Salby, 1997: The role of cloud diurnal variations in the time-mean energy budget. *J. Climate,* **10,** 1114–1124.

Chakraborty, A., and T. N. Krishnamurti, 2006: Improved seasonal climate forecasts of the South Asian summer monsoon using a suite of 13 coupled ocean–atmosphere models. *Mon. Wea. Rev.,* **134,** 1697–1721.

——, and ——, 2008: Improved forecasts of the diurnal cycle in the tropics using multiple global models. Part II: Asian summer monsoon. *J. Climate,* **21,** 4045–4067.

——, and ——, 2009: Improving global model precipitation forecasts over India using downscaling and the FSU superensemble. Part II: Seasonal climate. *Mon. Wea. Rev.,* **137,** 2736–2757.

——, ——, and C. Gnanaseelan, 2007: Prediction of the diurnal cycle using a multimodel superensemble. Part II: Clouds. *Mon. Wea. Rev.,* **135,** 4097–4116.

Charles, M. E., and B. A. Colle, 2009: Verification of extratropical cyclones within the NCEP operational models. Part I: Analysis errors and short-term NAM and GFS forecasts. *Wea. Forecasting,* **24,** 1173–1190.

Colle, B. A., C. F. Mass, and D. Ovens, 2001: Evaluation of the timing and strength of MM5 and Eta surface trough passages over the eastern Pacific. *Wea. Forecasting,* **16,** 553–572.

Dai, A., 2001: Global precipitation and thunderstorm frequencies. Part II: Diurnal variations. *J. Climate,* **14,** 1112–1128.

——, and C. Deser, 1999: Diurnal and semidiurnal variations in global surface wind and divergence fields. *J. Geophys. Res.,* **104,** 31 109–31 126.

——, F. Giorgi, and K. E. Trenberth, 1999: Observed and model-simulated precipitation diurnal cycle over the contiguous United States. *J. Geophys. Res.,* **104,** 6377–6402.

Druyan, L. M., M. Fulakeza, and L. Patric, 2002: Dynamical downscaling of seasonal climate predictions over Brazil. *J. Climate,* **15,** 84–117.

Harper, K., L. W. Uccellini, E. Kalnay, K. Carey, and L. Morone, 2007: 50th anniversary of numerical weather prediction. *Bull. Amer. Meteor. Soc.,* **88,** 639–650.

Huth, R., 2002: Statistical downscaling of daily temperature in central Europe. *J. Climate,* **15,** 1731–1742.

Janowiak, J. E., V. E. Kousky, and R. J. Joyce, 2005: Diurnal cycle of precipitation determined from the cmorph high spatial and temporal resolution global precipitation analysis. *J. Geophys. Res.,* **110,** D23105, doi:10.1029/2005JD006156.

Kalnay, E., S. J. Lord, and R. D. McPherson, 1998: Maturity of operational numerical weather prediction: Medium range. *Bull. Amer. Meteor. Soc.,* **79,** 2753–2769.

Krishnamurti, T. N., and C. M. Kishtawal, 2000: A pronounced continental-scale diurnal mode of the Asian summer monsoon. *Mon. Wea. Rev.,* **128,** 462–472.

——, C. Gnanaseelan, and A. Chakraborty, 2007: Prediction of the diurnal cycle using a multimodel superensemble. Part I: Precipitation. *Mon. Wea. Rev.,* **135,** 3613–3632.

——, A. K. Mishra, A. Chakraborty, and M. Rajeevan, 2009: Improving global model precipitation forecasts over India using downscaling and the FSU superensemble. Part I: 1–5-day forecasts. *Mon. Wea. Rev.,* **137,** 2713–2735.

Mass, C. F., D. Ovens, K. Westrick, and B. A. Colle, 2002: Does increasing horizontal resolution produce more skillful forecasts? *Bull. Amer. Meteor. Soc.,* **83,** 407–430.

McMurdie, L., and C. Mass, 2004: Major numerical forecast failures over the northeast Pacific. *Wea. Forecasting,* **19,** 338–356.

Murakami, M., 1983: Analysis of the deep convective activity over the tropical western Pacific. *J. Meteor. Soc. Japan,* **61,** 60–77.

Palmer, T. N., and Coauthors, 2004: Development of a European Multimodel Ensemble System for Seasonal to Interannual Prediction (DEMETER). *Bull. Amer. Meteor. Soc.,* **85,** 853–872.

Pandey, G. R., D. R. Cayan, M. D. Dettinger, and K. P. Georgakakos, 2000: A hybrid orographic plus statistical model for downscaling daily precipitation in northern California. *J. Hydrometeor.,* **1,** 491–506.

Randall, D. A., Harshvardhan, and D. A. Dazlich, 1991: Diurnal variability of the hydrologic cycle in a general circulation model. *J. Atmos. Sci.,* **48,** 40–62.

Shin, K.-S., G. R. North, Y.-S. Ahn, and P. A. Arkin, 1990: Time scales and variability of area-averaged tropical oceanic rainfall. *Mon. Wea. Rev.,* **118,** 1507–1516.

Simmons, A. J., and A. Hollingsworth, 2002: Some aspects of the improvement in skill of numerical weather prediction. *Quart. J. Roy. Meteor. Soc.,* **128,** 647–677.

Slingo, J. M., P. Inness, R. Neale, S. Woolnough, and G.-Y. Yang, 2003: Scale interactions on diurnal to seasonal timescales and their relevance to model systematic errors. *Ann. Geophys.,* **46,** 139–155.

Storch, H. V., H. Langenberg, and F. Feser, 2000: A spectral nudging technique for dynamical downscaling purposes. *Mon. Wea. Rev.,* **128,** 3664–3673.

Trenberth, K. E., A. Dai, R. M. Rasmussen, and D. B. Parsons, 2003: The changing character of precipitation. *Bull. Amer. Meteor. Soc.,* **84,** 1205–1217.

Wallace, J. M., 1975: Diurnal variations in precipitation and thunderstorm frequency over the conterminous United States. *Mon. Wea. Rev.,* **103,** 403–419.

Wedam, G. B., L. A. McMurdie, and C. F. Mass, 2009: Comparison of model forecast skill of sea level pressure along the east and west coasts of the United States. *Wea. Forecasting,* **24,** 843–854.

Yang, G.-Y., and J. Slingo, 2001: The diurnal cycle in the tropics. *Mon. Wea. Rev.,* **129,** 784–801.

Yang, S., and E. A. Smith, 2006: Mechanisms for diurnal variability of global tropical rainfall observed from TRMM. *J. Climate,* **19,** 5190–5226.